# AB-INITIO AND DENSITY FUNCTIONAL THEORY SIMULATION FOR LACTIDE MONOMER

Mohamed ELDESSOUKI[1,2*], Yasser GOWAYED[3], Orlando ACEVEDO[4]

*[1)] Department of Materials Engineering, Technical University of Liberec, Liberec, Czech Republic*

*[2)] Department of Textile Engineering, Mansoura University, Mansoura, Egypt*

*[3)] Department of Polymer and Fiber Engineering, Auburn University, Auburn, AL, USA*

*[4)] Department of Chemistry & Biochemistry, Auburn University, Auburn, AL, USA*

*[*)] Corresponding author: mohamed.eldessouki@tul.cz*

**Abstract**

Poly(L-lactide) is one of the polyesters that are widely used in fibrous, packaging and biomedical applications. The modeling in this work aimed to simulate the properties of the lactide monomer as well as the produced polymer with an emphasis on the properties that can be experimentally verified. Simulations were performed at electronic scale by implementing different methods that represent multiple levels of the theory. Comparing the simulation results with the experimental data obtained from X-ray single crystallography showed that low level methods such as Hartree-Fock (HF) were able to optimize and predict the geometry of molecules with accuracy higher than that obtained with density functional theory (DFT) methods which performed better in predicting the energy and the spectroscopic (IR and NMR) properties for the structures. Increasing the size of the basis sets with DFT did not show much improvement in the prediction accuracy beyond a certain limit and B3LYP/6-311+G(2d,p) method was found to be sufficient for the calculation.

**Keywords:** Density Functional Theory; Hartree-Fock calculation; Poly(L-Lactide); Spectroscopic properties; X-ray crystallography

## 1. INTRODUCTION

Poly (L-lactide) is a biocompatible and bioresorbable polyester that is widely used in biomedical applications [1] as a homopolymer or in a mix with other polymers. These biomedical applications extend from orthopedic fixation devices [2], wound resorbable sutures [3], artificial skin [4], stents [5], controlled drug delivery [6], to tissue engineering [7]. PLA polymerization can be achieved by a lactic acid poly-condensation reaction or through the ring opening polymerization (ROP) of lactide monomers. The ROP reaction is driven by the reduction of the total free energy of the molecule as a result of the relief of the conformation strains in the cyclic monomers [8]. The ROP reaction is preferred in producing PLA as it provides better control over the molecular weight of final polymer [9], [10].

Multiscale modeling and simulation is widely applied for polymeric systems to predict many of their properties based on the knowledge of the chemical structure only [11]. Multiscale methods [12] range from electronic/quantum scale [13], [14], atomistic/molecular scale [15], [16], meso/micro scale [12], and continuum/macro scale [17]. The advantage of using the electronic (e.g. *ab initio*, density functional theory) and molecular (e.g., molecular dynamics, Monte Carlo) modeling scales is that they provide the ability to understand the behavior of the material bottom-up through the primitive and basic elements of the material. Also, some of these methods do not need any input from experiments to predict material properties, and they allow the simulation for systems under controlled and/or inaccessible conditions [18].

Some properties of PLA were modeled in the literature [19]–[22] at the molecular scale where molecular dynamics (MD) is usually used. Zhang *et al.* [20] used MD simulation to study the effect of the molecular weight of PLA on its predicted glass transition temperature, self-diffusion coefficient and shear viscosity.

The electronic/quantum scale simulation including *ab initio* and density functional theory (DFT) methods was implemented in the literature to study different structural properties of polymers. For example, quantum-based methods were used to study the mechanisms of free radical polymerization and to calculate the kinetics of the reaction with determination of the reaction rates for individual reaction steps [13]. DFT-based calculations were used to trace the changes in the surface electronic structure and energy of fuel cell components [14]. They were used to study the geometric and electronic properties of polyacetylene molecule in different ionic states (neutral, cationic, and anionic) with the influence of external electric field [15].

Atomistic models implementing molecular dynamic (MD) simulation are widely used in studying polymeric systems to predict some of their macroscopic properties such as glass transition temperatures [1], density and solubility parameters of ionic liquids [16], elastic properties[17], gas permeability in amorphous polymers[18]. They were also applied with branched polymers to determine the effect of modifying the terminal group on the solution properties of the dendrimers [19]. MD simulation was used to study the local and chain dynamics of a polymer melt as well as its thermodynamic and static properties [20], and some other properties such as shear yielding, creep, physical aging, strain hardening and crazing [21].

This work aims at implementing the principles of molecular modeling to theoretically study and model the lactide monomer through its synthesized polymer with an emphasis on the properties that feasibly be verified experimentally. Geometry optimization and energy calculation of lactide monomer and oligomer was performed using electronic simulation methods. Spectroscopic properties (IR and NMR) were also predicted and compared with the experiments.

## 2. Materials and Methods

### *2.1. Systems of study*

The electronic modeling calculations were performed to study two systems of the lactide monomer (molecular weight of 144.13 g/mole) and the oligomers with two open lactide rings. The oligomer consists of four repeat units with a total molecular weight of 334.32 g/mole after the addition of the ethanol to the beginning of the chain as it initiates the ring opening. The electronic simulations were performed using the Hartree-Fock (HF) method [22] as well as the density functional theory where different levels of the theory were applied. All electronic modeling calculations were performed using Gaussian 09 software [23].

### 2.2. Hartree-Fock calculations

Based on the principles of quantum mechanics, the energy and other related properties of a molecule may be obtained by solving the Schrödinger equation:

$$\hat{\mathcal{H}}\Psi = E\Psi \tag{1}$$

Where: $\Psi$ is the wavefunction, $\hat{H}$ is the Hamiltonian operator that can be expressed as:

$$\hat{\mathcal{H}} = \sum_{i=1}^{2n} -\frac{1}{2}\nabla_i^2 - \sum_{\text{all } \mu,i} \frac{Z_\mu}{r_{\mu i}} + \sum_{\text{all } i,j} \frac{1}{r_{ij}} \tag{2}$$

Which represents the summations of (from left to right) electron kinetic energy terms, nucleus-electron attraction potential energy terms, and electron–electron repulsion potential energy terms. The energy levels of the molecule *E* can be calculated by finding the eignvalues of the system as:

$$E = \frac{\int \Psi^* \hat{\mathcal{H}} \Psi \, d\tau}{\int \Psi^* \Psi \, d\tau} \tag{3}$$

The Hartree-Fock (HF) method can computationally solve this equation which can turn, after some tedious algebraic manipulations, to the following expression:

$$E = 2\sum_{i=1}^{n} H_{ii} + \sum_{i=1}^{n}\sum_{j=1}^{n}(2J_{ij} - K_{ij}) \quad (4)$$

With; $H_{ii}$ representing the electronic energy (including the $\widehat{H}^{core}$ operator), $J_{ij}$ the coulomb integral, and $K_{ij}$ the exchange integral. To use this method to solve the Schrödinger equation for molecules, basis functions are required to mathematically represent the molecular orbitals within a molecule. The size of the applied basis sets determines the accuracy of this mathematical representation as well as the resources required to solve the problem. In this work, different basis sets were applied during the simulation where the 6-31G(d) basis set was used for the HF low level calculations. This basis set includes six primitive base functions of Gaussian type that were used with a double zeta split on the valence shell and with polarized basis set of d type applied for every heavy atom [24].

Hartree-Fock method was applied to optimize the structures of the lactide monomer and the PLA oligomer. Frequency analysis was then performed on the optimized structures to obtain their IR spectra, zero point energy (ZPE), and to check the state of the optimized structures to determine if they are minimum points on the potential energy surface (PES) or they are saddle points [25]. Finally, NMR calculation procedure was applied on the optimized structures to produce their NMR spectra.

### 2.3. Density functional theory

In the previously described Hartree-Fock and other *ab initio* methods, most of the calculations are required to determine the wavefunctions for the molecules while these wavefunctions neither exist physically nor can be measured. Therefore, density functional theory (DFT) was introduced based on the electron probability density function $\rho(x,y,z)$ which can be measured using X-ray or electron diffractions [26]. DFT provides the results quality for some computationally expensive *ab initio* methods with the low resources required for HF method [26, 27]. The method of Kohn-Sham (KS) self consistent equations [28] is implemented in the DFT calculations and can be expressed as:

$$\left[-\frac{1}{2}\nabla_i^2 - \sum_{\text{nuclei A}} \frac{Z_A}{r_{1A}} + \int \frac{\rho(r_2)}{r_{12}}\, dr_2 + \upsilon_{XC}(1)\right]\Psi_i^{KS}(1) = \epsilon_i^{KS}\Psi_i^{KS}(1) \quad (5)$$

Where $\Psi^{KS}$ is the KS spatial orbitals, and $\upsilon_{xc}(r)$ is the exchange correlation potential which can be expressed as:

$$\upsilon_{XC}(r) = \frac{\delta\, E_{XC}[\rho(r)]}{\delta\, \rho(r)} \quad (6)$$

The exchange-correlation energy functional $E_{xc}[\rho(r)]$ has different forms, among them is the B3LYP which includes Beck3 exchange function with the Lee–Yang–Parr (LYP) correlation function (hence, assigned the name B3LYP) [29]. B3LYB is a hybrid functional with terms calculated from the HF theory and others based on the DFT and can be expressed as:

$$E_{XC}^{B3LYP} = (1 - a_0 - a_x)E_X^{LSDA} + a_0 E_X^{HF} + a_x E_X^{B88} + (1 - a_c)E_c^{VWN} + a_c E_c^{LYP} \quad (7)$$

In the current work, a sequence of optimization, frequency analysis, and NMR analysis was performed on the lactide monomers and oligomers using the DFT higher level calculations. Three basis sets were applied during the calculations where 6-311G(d) basis set was applied (calculations were assigned the name DFT-1) with triple split in the valence shell. The second basis set (assigned the name DFT-2) was the 6-311+G(2d,p) where diffusion functions were applied on heavy atoms and two polarized functions of d type were applied on heavy atoms and one polarized function of p type was applied on hydrogen atoms of the simulated structure.

The third (assigned the name DFT-3) basis set was the 6-311++G(3df,3pd) where extra diffusion and polarization were considered for hydrogen atoms [24].

### 2.4. X-ray single crystallography

To measure the exact geometry of the lactide monomer for comparing with the geometries obtained from the simulations, X-ray single crystallography was conducted on a Bruker SMART APEX diffractometer. The instrument is a charge-coupled device (CCD) with area-detector equipped with monochromated MoKa, with a wave length λ = 0.71073 Å and operated at 2 KW power (50 kV, 40 mA).The X-ray intensities were measured at temperature of 273(2) K. The unit cell parameters were adjusted to have orthorhombic cell, space group P21. Cell dimensions were a = 9.2653(6) Å, b = 13.4991(8) Å, c = 16.7023(10) Å, angles were set to α = β = γ= 90˚, volume = 2089.0(2) $Å^3$, and Z = 12. The absorption correction coefficient μ = 0.117 $mm^{-1}$. A total of 5,172 frames were collected during the sample run. The structure was solved by direct methods and the subsequent difference Fourier syntheses on SHELXS-97 and refined with the SHELXL-97 software package.

## 3. RESULTS AND DISCUSSION

### 3.1. Geometry optimization and energy calculations

The geometry of the lactide monomer was optimized at different levels of the theory using HF and DFT with different basis sets as described before. Geometries of the optimized structures were compared to the experimental geometry obtained from the X-ray single crystallography which is shown in Figure 1. The root mean square error (RMSE) was used as an indicator for the convergence or divergence of the optimized structures from the actual structure obtained from the experiments. The RMSE can be expressed as:

$$RMSE = \sqrt{\frac{\sum(\vec{r_i} - \vec{r_0})^2}{N}} \quad (8)$$

Where; $\vec{r_i}$ refers to the vector of optimized values for the measured property (i.e. bond, angle, or dihedral), $\vec{r_0}$ is the vector for the corresponding experimental values, and N is the number of readings for each property.

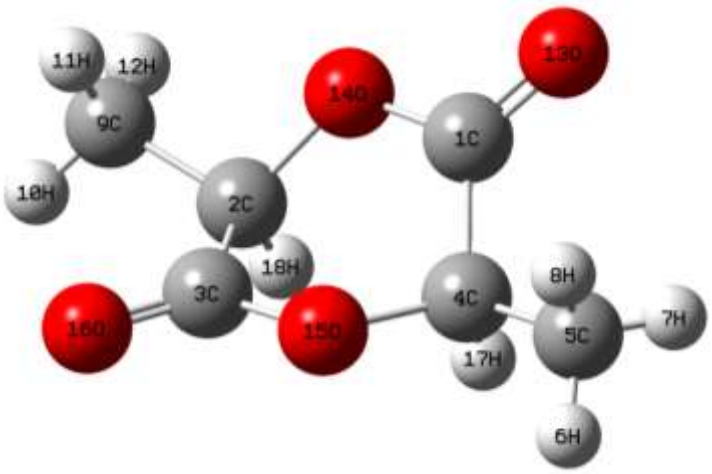


**Figure 1.** The structure of the lactide monomer as obtained from the X-ray single crystallography

The bond lengths, angles, and dihedrals for the experimental structure as well as the structures obtained from the different optimization methods are given in Table 1 in the form of Z-matrices. The RMSE value for each method is also given at the last two rows of the table. Based on the results given in Table 1, it is noticed that the low level calculation using HF method is able to predict the geometry of the structure

reasonably with accuracy higher than other methods. This high accuracy is indicated with the low RMSE for HF methods in bond lengths and dihedrals. The RMSE was generally high for dihedrals with all methods which can be attributed to the sign change in the dihedral angle for oxygen atom (number 14) and the hydrogen atom (number 6), although the HF calculation was able to predict the correct sign for the last atom. These results agree with the known ability of HF method to predict the geometry [24, 37] although HF may not be the best choice for calculating the energy of the molecule. The reason for HF to have a high deviation from the experimental value for the energy is the lack of calculating the electron-electron interaction during the calculation [24].

On the other hand, the molecular energy calculated with DFT methods show a reasonable agreement with the energy calculated for the structure obtained from the X-ray experiment. This result indicates that DFT is not sensitive to the level of geometry optimization and it is robust to calculate the energy of the molecule with little geometry inaccuracy. Results also show that computationally expensive methods are not usually the most accurate ones and an increase in the number of basis sets may not have the same weight in optimizing the geometry as it does in calculating the energy of the molecule.

**Table 1.** Geometries of the experimental and the optimized lactide monomer

| Atom# | Symbol | NA | NB | NC | Experimental (X-rays) | | | Predicted using HF | | | Predicted using DFT-1[a] | | | Predicted using DFT-2[b] | | | Predicted using DFT-3[c] | | |
|---|---|---|---|---|---|---|---|---|---|---|---|---|---|---|---|---|---|---|---|
| | | | | | Bond (Å) | Angle (˚) | Dihedral (˚) | Bond (Å) | Angle (˚) | Dihedral (˚) | Bond (Å) | Angle (˚) | Dihedral (˚) | Bond (Å) | Angle (˚) | Dihedral (˚) | Bond (Å) | Angle (˚) | Dihedral (˚) |
| 1 | C | | | | | | | | | | | | | | | | | | |
| 2 | C | 1 | | | 2.39* | | | 2.38 | | | 2.41 | | | 2.41 | | | 2.41 | | |
| 3 | C | 2 | 1 | | 1.50 | 88.28 | | 1.52 | 89.58 | | 1.53 | 89.53 | | 1.53 | 89.47 | | 1.53 | 89.48 | |
| 4 | C | 1 | 2 | 3 | 1.51 | 82.37 | 40.87 | 1.52 | 84.07 | 33.70 | 1.53 | 82.99 | 36.70 | 1.53 | 83.18 | 36.40 | 1.53 | 83.23 | 36.24 |
| 5 | C | 4 | 1 | 2 | 1.49 | 113.63 | -167.36 | 1.51 | 112.77 | -161.98 | 1.51 | 112.95 | -164.06 | 1.51 | 113.07 | -163.99 | 1.51 | 113.03 | -163.84 |
| 6 | H | 5 | 4 | 1 | 0.96 | 109.56 | 177.26 | 1.08 | 109.38 | 179.91 | 1.09 | 109.84 | -179.34 | 1.09 | 109.70 | -179.06 | 1.09 | 109.70 | -179.09 |
| 7 | H | 5 | 4 | 1 | 0.96 | 109.47 | -62.72 | 1.08 | 109.97 | -59.85 | 1.09 | 109.97 | -59.03 | 1.09 | 109.73 | -58.88 | 1.09 | 109.71 | -58.91 |
| 8 | H | 5 | 4 | 1 | 0.96 | 109.52 | 57.20 | 1.08 | 110.30 | 60.07 | 1.09 | 110.47 | 60.46 | 1.09 | 110.49 | 60.61 | 1.09 | 110.46 | 60.57 |
| 9 | C | 2 | 1 | 4 | 1.51 | 136.35 | 162.43 | 1.51 | 136.19 | 157.17 | 1.51 | 136.59 | 160.67 | 1.51 | 136.68 | 160.55 | 1.51 | 136.64 | 160.30 |
| 10 | H | 9 | 2 | 1 | 0.96 | 109.45 | -174.05 | 1.08 | 109.97 | -175.07 | 1.09 | 109.97 | -174.79 | 1.09 | 109.73 | -174.80 | 1.09 | 109.71 | -174.73 |
| 11 | H | 9 | 2 | 1 | 0.96 | 109.46 | -54.10 | 1.08 | 110.30 | -55.15 | 1.09 | 110.47 | -55.30 | 1.09 | 110.49 | -55.31 | 1.09 | 110.46 | -55.26 |
| 12 | H | 9 | 2 | 1 | 0.96 | 109.51 | 65.94 | 1.08 | 109.38 | 64.69 | 1.09 | 109.84 | 64.90 | 1.09 | 109.70 | 65.02 | 1.09 | 109.70 | 65.08 |
| 13 | O | 1 | 4 | 5 | 1.20 | 124.76 | 13.31 | 1.18 | 123.70 | 24.15 | 1.20 | 124.18 | 19.95 | 1.20 | 124.18 | 20.23 | 1.20 | 124.24 | 20.36 |
| 14 | O | 1 | 13 | 4 | 1.34 | 120.24 | 177.80 | 1.33 | 121.52 | -179.55 | 1.35 | 121.11 | -179.78 | 1.35 | 120.92 | -179.61 | 1.35 | 121.00 | -179.58 |
| 15 | O | 3 | 2 | 1 | 1.34 | 115.64 | -19.84 | 1.33 | 114.78 | -15.05 | 1.35 | 114.70 | -18.49 | 1.35 | 114.89 | -18.24 | 1.35 | 114.76 | -18.21 |
| 16 | O | 3 | 2 | 1 | 1.20 | 124.63 | 158.03 | 1.18 | 123.70 | 165.38 | 1.20 | 124.18 | 161.71 | 1.20 | 124.18 | 162.13 | 1.20 | 124.24 | 162.18 |
| 17 | H | 4 | 1 | 13 | 0.98 | 109.17 | -108.76 | 1.09 | 107.63 | -97.28 | 1.10 | 107.77 | -101.74 | 1.10 | 107.50 | -101.30 | 1.10 | 107.40 | -101.05 |
| 18 | H | 2 | 1 | 13 | 0.98 | 97.69 | 110.17 | 1.09 | 97.12 | 95.19 | 1.10 | 96.37 | 101.67 | 1.10 | 96.43 | 101.31 | 1.10 | 96.62 | 101.31 |
| **RMSE** | | | | | **0** | **0** | **0** | **0.08** | **0.94** | **92.51** | **0.09** | **0.83** | **130.45** | **0.09** | **0.82** | **130.38** | **0.09** | **0.82** | **130.38** |
| **Energy of the molecule (Hartree)** | | | | | **-534.432** | | | **-531.339** | | | **-534.497** | | | **-534.534** | | | **-534.561** | | |

* This value refers to the distance between atoms #1 and #2 while there is no bond between these atoms.
[a] Values as obtained from DFT calculation using 6-311G(d) basis set.
[b] Values as obtained from DFT calculation using 6-311+G(2d,p) basis set.
[c] Values as obtained from DFT calculation using 6-311++G(3df,3pd) basis set.

Results of different calculation methods as well as the experiments show that an equatorial conformation of the pendent methyl groups was preferred in the lactide monomer. To verify this result a scan for the potential energy surface (PES) was performed by changing the angle of the pendent methyl groups from axial conformation to equatorial conformation. The DFT-1 calculation method was applied during this scan to optimize and calculate the energy of the molecule as it was found in the previous results to be an efficient

method. Results for this scan are shown in Figure 2 which indicates a high energy of the molecule in the case of axial conformation (steps No. 1 to 4 in the figure) while this energy was decreased and the molecule became more stable after changing to the equatorial conformation (steps No. 6 and 7 on the graph). The lactide was also observed in the experimental results as well as the optimized structures to have the boat conformer as a stable conformation. This conformation is unlike the preferred chair conformer for other six member rings such as cyclohexane [38]. The reasons for the instability of chair over the boat conformation might be attributed to the larger deformations of valence angles and torsional strains in the case of lactide chair conformation [39].

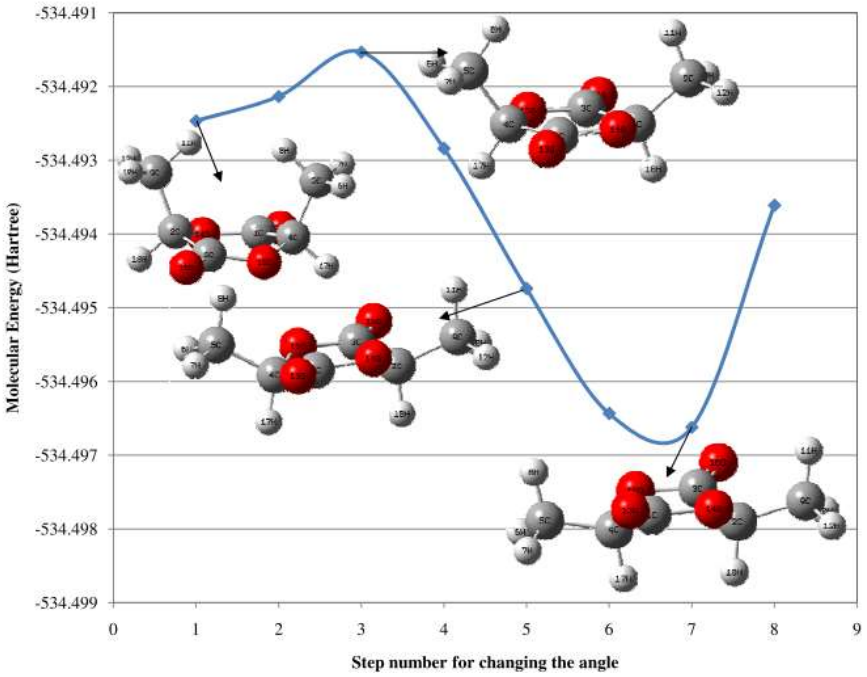


**Figure 2.** Potential energy surface (PES) scan for the change in the molecular energy with the change in the conformation of pendent methyl group from axial to equatorial

### 3.2. IR and NMR spectroscopy

The predicted IR vibrational spectrum for the lactide monomer is shown at the lower part of Figure 3 as compared to the experimental spectrum of the molecule shown at the top part of the figure. The given spectrum was calculated using DFT-3 calculation (with the highest basis sets) and it was the closest to the experiment even without the application of the correction factors. The other calculated spectra showed the same general trend of peaks but with shifting of the peak at *ca.* 1750 $cm^{-1}$ toward higher values. These peak shifts may lie in an acceptable range from the experimental values after the application of the recommended correction factors [24]. The spectrum of the lactide oligomer is shown in the lower part of Figure 4 as calculated from DFT-2 method and compared to the experimental spectrum of PLA in the same figure. The calculated spectrum showed a doublet peak for the carbonyl group at *ca.* 1750 $cm^{-1}$ which was also noticed in the results of the other calculation methods.

Investigating the double peak behavior in the calculated spectra indicates two vibrational modes for the carbonyl groups based on their position in the chain. Carbonyl groups that are located closer to the end of the chain showed different frequency than the groups located on the backbone of the chain which results of this double peak. Also, since the simulation was performed on a small molecule (oligomer) the peak strength was close for both modes especially when compared to the tested polymer which has a relatively higher molecular weight that weaken this effect.

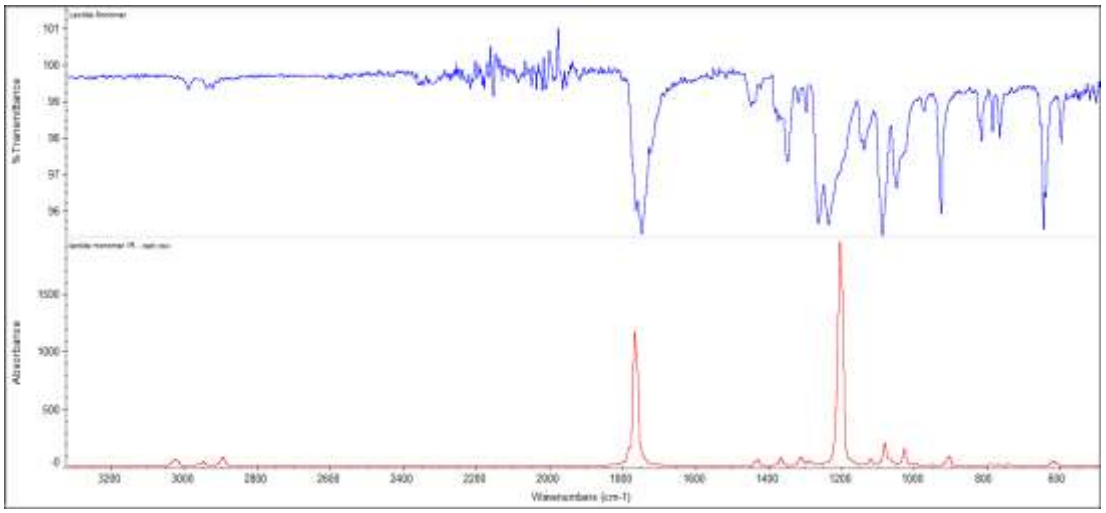

Figure 3. FTIR spectra for the lactide monomer as measured experimentally (top) and as predicted from DFT-3 calculations (bottom)

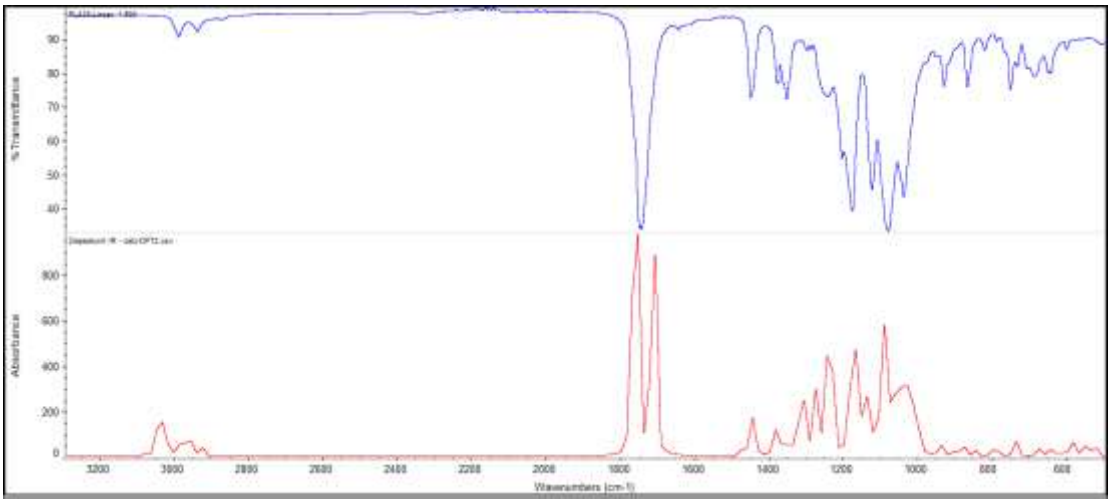

Figure 4. The measured FTIR spectrum for PLA (top) and the predicted spectrum of the PLA oligomer (bottom)

The predicted proton nuclear magnetic resonance ($^1$H NMR) spectrum for lactide monomer is shown in Figure 5 which is reasonably comparable to the experimental spectrum of the molecule shown in Figure 6. The calculated spectra predicted the chemical shift $\delta \approx 1.8$ for the six protons on the two methyl groups, as shown by degeneracy value of 2 with three peaks. The chemical shift at $\delta \approx 5.1$ corresponds to the protons on the alpha carbons in the molecule.

The spectrum of the lactide oligomer as obtained from the simulation predicted peaks in a reasonably agreement with the chemical shift values obtained from the experiments. The small number of repeat units during the simulation (four repeat units), however, made it hard to show the comparison with the actual polymer with high molecular weight (more repeat units). Based on the obtained results, DFT calculation methods performed better than the HF method in predicting the IR and NMR spectra for the monomer as well as the oligomer and the accuracy increased with the size of the basis set giving a better match in the following order: DFT-3 > DFT-2 > DFT-1 > HF.

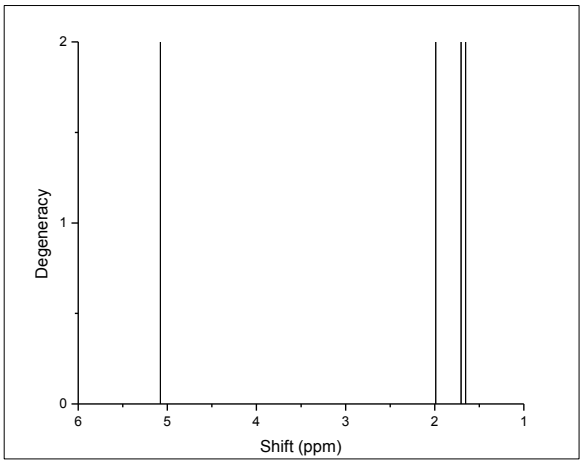


**Figure 5.** $^{1}$H NMR spectrum for lactide monomer calculated using DFT-3

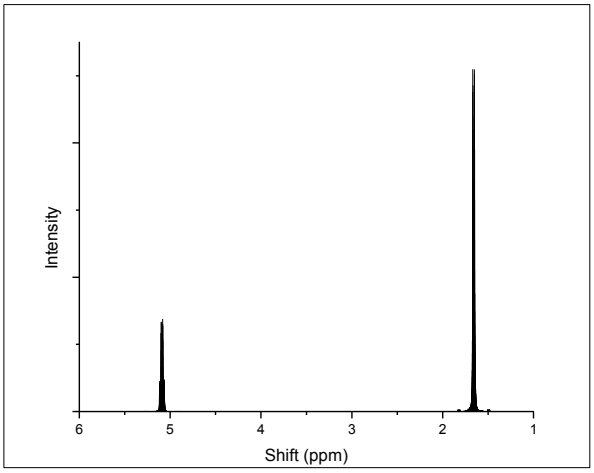


**Figure 6.** The measured $^{1}$H NMR spectrum for the lactide monomer

## CONCLUSION

Modeling of lactide monomer was performed at the electronic scale and different properties were predicted from the simulation. Results of the geometrical and structural properties were compared to experimental measurements obtained from the X-ray single crystallography. It was found that the low level calculation using HF/6-31G(d) method was able to successfully simulate the correct geometry of the molecules with accuracy higher than that obtained from DFT methods. HF method, however, was not able to accurately calculate the energy of the molecule compared to DFT methods. It was also observed that DFT methods are insensitive to the accuracy of the geometry of the structure and the results of using low basis set size were as good as using high basis set size. Results suggest that a B3LYP / 6-311+G(2d,p) method is sufficient to optimize the structure and to calculate its energy and its vibrational frequencies. Increasing the size of the basis set beyond that limit was not significantly effective in increasing the accuracy of the results. The lactide molecule was found to prefer the boat conformation which is more stable than chair conformation due to the high torsion strains and valence angles in the chair conformation. The electronic simulation methods were successful in predicting the IR and NMR spectra of the molecules and the DFT methods were able to resemble experimental spectra even without the application of correction factors. The relatively accurate results for the simulation methods introduced in this work indicate that these methods can be trusted to calculate many of the polymer properties using the computer (*in silico*). This will be beneficial in designing new products as it saves a lot of the laborious work associated with the production and testing of materials.

**ACKNOWLEDGEMENTS**

***This work was supported by ESF operational program "Education for Competitiveness" in the Czech Republic in the framework of project "Support of engineering of excellent research and development teams at the Technical University of Liberec" No. CZ.1.07/2.3.00/30.0065.***

**REFERENCES:**

[1] A.-C. Albertsson and I. K. Varma, "Recent developments in ring opening polymerization of lactones for biomedical applications," *Biomacromolecules*, vol. 4, no. 6, pp. 1466–1486, 2003.

[2] J. W. Leenslag, A. J. Pennings, R. R. M. Bos, F. R. Rozema, and G. Boering, "Resorbable materials of poly (L-lactide). VI. Plates and screws for internal fracture fixation," *Biomaterials*, vol. 8, no. 1, pp. 70–73, 1987.

[3] R. S. Bezwada, D. D. Jamiolkowski, I.-Y. Lee, V. Agarwal, J. Persivale, S. Trenka-Benthin, M. Erneta, J. Suryadevara, A. Yang, and S. Liu, "Monocryl® suture, a new ultra-pliable absorbable monofilament suture," *Biomaterials*, vol. 16, no. 15, pp. 1141–1148, 1995.

[4] S. Gogolewski and A. J. Pennings, "An artificial skin based on biodegradable mixtures of polylactides and polyurethanes for full-thickness skin wound covering," *Die Makromol. Chemie, Rapid Commun.*, vol. 4, no. 10, pp. 675–680, 1983.

[5] H. Tamai, K. Igaki, E. Kyo, K. Kosuga, A. Kawashima, S. Matsui, H. Komori, T. Tsuji, S. Motohara, and H. Uehata, "Initial and 6-month results of biodegradable poly-l-lactic acid coronary stents in humans," *Circulation*, vol. 102, no. 4, pp. 399–404, 2000.

[6] S. Y. Kim, I. G. Shin, and Y. M. Lee, "Preparation and characterization of biodegradable nanospheres composed of methoxy poly(ethylene glycol) and dl-lactide block copolymer as novel drug carriers," *J. Control. Release*, vol. 56, no. 1–3, pp. 197–208, Dec. 1998.

[7] S. L. Ishaug-Riley, G. M. Crane-Kruger, M. J. Yaszemski, and A. G. Mikos, "Three-dimensional culture of rat calvarial osteoblasts in porous biodegradable polymers," *Biomaterials*, vol. 19, no. 15, pp. 1405–1412, 1998.

[8] G. G. Odian and G. Odian, *Principles of polymerization*, vol. 3. Wiley-Interscience New York, 2004.

[9] R. Mehta, V. Kumar, H. Bhunia, and S. N. Upadhyay, "Synthesis of poly (lactic acid): a review," *J. Macromol. Sci. Part C Polym. Rev.*, vol. 45, no. 4, pp. 325–349, 2005.

[10] C. Jérôme and P. Lecomte, "Recent advances in the synthesis of aliphatic polyesters by ring-opening polymerization," *Adv. Drug Deliv. Rev.*, vol. 60, no. 9, pp. 1056–1076, 2008.

[11] J. Han, R. H. Gee, and R. H. Boyd, "Glass transition temperatures of polymers from molecular dynamics simulations," *Macromolecules*, vol. 27, no. 26, pp. 7781–7784, 1994.

[12] Q. H. Zeng, A. B. Yu, and G. Q. Lu, "Multiscale modeling and simulation of polymer nanocomposites," *Prog. Polym. Sci.*, vol. 33, no. 2, pp. 191–269, 2008.

[13] R. Resta, "Ab initio simulation of the properties of ferroelectric materials," *Model. Simul. Mater. Sci. Eng.*, vol. 11, no. 4, p. R69, 2003.

[14] A. E. Mattsson, P. A. Schultz, M. P. Desjarlais, T. R. Mattsson, and K. Leung, "Designing meaningful density functional theory calculations in materials science—a primer," *Model. Simul. Mater. Sci. Eng.*, vol. 13, no. 1, p. R1, 2005.

[15] W. A. Curtin and R. E. Miller, "Atomistic/continuum coupling in computational materials science," *Model. Simul. Mater. Sci. Eng.*, vol. 11, no. 3, p. R33, 2003.

[16] V. A. Harmandaris, V. G. Mavrantzas, and D. N. Theodorou, "Atomistic molecular dynamics simulation of stress relaxation upon cessation of steady-state uniaxial elongational flow," *Macromolecules*, vol. 33, no. 21, pp. 8062–8076, 2000.

[17] J. Yanagimoto, "FE-based analysis for the prediction of inner microstructure in metal forming," *Model. Simul. Mater. Sci. Eng.*, vol. 10, no. 6, p. R111, 2002.

[18] M. Laso and E. A. Perpète, *Multiscale modelling of polymer properties*. Elsevier Amsterdam, 2006.

[19] M. Liu, M. Pu, and H. Ma, "Molecular dynamics simulation of polylactic acid/ organoclay nanocomposites: Effects of different organic modifiers," *Nanoelectronics Conference (INEC), 2010 3rd International*. pp. 148–149, 2010.

[20] J. Zhang, Y. Liang, J. Yan, and J. Lou, "Study of the molecular weight dependence of glass transition temperature for amorphous poly(l-lactide) by molecular dynamics simulation," *Polymer (Guildf).*, vol. 48, no. 16, pp. 4900–4905, Jul. 2007.

[21] J. Zhang, J. Lou, S. Ilias, P. Krishnamachari, and J. Yan, “Thermal properties of poly(lactic acid) fumed silica nanocomposites: Experiments and molecular dynamics simulations,” *Polymer (Guildf).*, vol. 49, no. 9, pp. 2381–2386, Apr. 2008.

[22] S.-Q. Zhou, X.-C. Cheng, Y.-L. Jin, J. Wu, and D.-S. Zhao, “Molecular dynamics simulation on interacting and mechanical properties of polylactic acid and attapulgite(100) surface,” *J. Appl. Polym. Sci.*, vol. 128, no. 5, pp. 3043–3049, Jun. 2013.